Greensphere:
Journal of Environmental Chemistry
ISSN: 2777-0664
Original Article

Effect of CTAB Templating on Mesoporous SiO_2 from Rice Husk on the Adsorption of Methylene Blue

Melisa Nur Kibtiah[1]*, Rahmad Nuryanto[1], Yayuk Astuti[1]
[1]Department of Chemistry, Faculty of Sciences and Mathematics, Diponegoro University, Semarang 50275, Indonesia

*Corresponding author: melisanurkibtiah@students.undip.ac.id

Received: 06 Maret 2026 / Accepted: 28 Mei 2026
Available online: 31 Mei 2026

Abstract

Water contamination caused by dye-containing industrial effluents remains a significant environmental concern, necessitating the development of efficient and sustainable treatment technologies. This study investigated the effect of cetyltrimethylammonium bromide (CTAB) as a structure-directing agent on the meso-structural properties and adsorption performance of rice husk-derived mesoporous $Si0_2$ toward methylene blue (MB). Mesoporous silica was synthesized hydrothermally using sodium silicate extracted from rice husk, both in the absence and presence of CTAB, yielding materials denoted as MS and MS-CTAB, respectively. Structural characterization revealed that CTAB-assisted synthesis significantly enhanced the textural properties of the material, resulting in a higher specific surface area (580.38 m^2/g) compared to MS (89.63 m^2/g), along with improved pore uniformity and accessibility. These structural improvements facilitated superior adsorption performance, with MS-CTAB achieving an MB removal efficiency of 86.02 %, compared to 74.19 % for MS. Adsorption kinetics were better described by the pseudo-second-order model, while equilibrium data were more accurately fitted by the Langmuir isotherm model, with a maximum adsorption capacity of 63.29 mg/g. The findings demonstrate that CTAB-assisted hydrothermal synthesis effectively improves the mesostructural characteristics and adsorption efficiency of rice husk-derived $Si0_2$, highlighting its potential as a sustainable adsorbent for dye removal from aqueous media.

Keywords: Template; Adsorption; Silica; Mesoporous

1. Introduction

Water pollution caused by the discharge of synthetic dyes from industrial activities remains a major challenge in environmental management [1]. Methylene blue (MB), a cationic dye commonly detected in wastewater from textile, pharmaceutical, and laboratory industries, is chemically stable and resistant to biodegradation, posing significant risks to aquatic ecosystems and human health [2]. The presence of MB in water bodies reduces light penetration, inhibits photosynthesis in aquatic organisms, and may accumulate within the food chain. Among the available treatment technologies, adsorption has been widely employed due to its high removal efficiency, operational simplicity, and relatively low cost compared to other separation methods [3].

Mesoporous silica has emerged as a promising adsorbent due to its high specific surface area, large pore volume, high thermal stability, and ease of surface modification [4,5] Its adsorption performance is strongly influenced by mesostructural regularity, pore size distribution, and the accessibility of active sites on the surface [4]. The development of these structural characteristics is largely governed by the synthesis strategy, particularly the choice of silica precursor, reaction conditions, and the use of structure-directing agents such as cetyltrimethylammonium bromide (CTAB), which facilitates the self-assembly of surfactant micelles and silicate species during pore network formation [5,6].

Subhan *et al.* [7] reported the synthesis of micro-mesoporous silica from a silica–alumina source derived from ZSM-5 zeolite using alkaline dissolution, CTAB-assisted self-assembly, and hydrothermal treatment at 110 ℃ for 24 h. The resulting material exhibited ordered pore structures and high MB adsorption capacity, confirming the effectiveness of CTAB in enhancing pore accessibility and adsorbent–adsorbate interactions. The synthesis relied on commercial precursors with highly controlled composition and purity, while the

effectiveness of CTAB templating in biomass-derived silica precursors with heterogeneous composition, residual mineral impurities, and varying silicate polymerization remains insufficiently understood. The use of alkaline dissolution, sulfuric acid-assisted pH adjustment, and relatively high-temperature hydrothermal treatment also increased process complexity, energy demand, and production costs. The present study addresses these limitations by employing rice husk-derived sodium silicate as a renewable silica precursor and applying hydrothermal synthesis at a lower temperature (100 ℃) without re-dissolution of commercial silica, providing a simpler and more sustainable approach for mesoporous silica formation.

Ali *et al.* [8] demonstrated that $Fe_3O_4 - SiO_2$ composite materials exhibit high MB adsorption efficiency, with a specific surface area reaching 385 m^2/g, through magnetic nanoparticle synthesis via a solvothermal method followed by silica coating using a modified Stöber method based on tetraethyl orthosilicate (TEOS). The study confirmed that surface area and pore volume are key textural parameters influencing adsorption capacity. The synthesis strategy relied on high-purity organo-silicate precursors, organic solvents such as ethanol, repeated centrifugation steps, and magnetic nanoparticle preparation, resulting in increased material costs and operational complexity. The investigation focused primarily on the adsorption performance of the final composite without specifically examining mesoporous SiO_2 formation or the contribution of templating agents to pore structure development. The relationship between CTAB-induced textural modification and adsorption enhancement therefore remained unclear. The present study employs biomass-derived SiO_2 as a single-component adsorbent, enabling a more direct evaluation of CTAB effects on surface area, pore size distribution, and adsorption capacity through a simpler and more sustainable synthesis approach.

Kim and An [9] reported the synthesis of $Fe_3O_4@SiO_2$ core–shell nanoparticles by varying the CTAB-to-TEOS ratio to control silica shell thickness and porosity. Increased CTAB content enhanced shell porosity without significantly affecting layer thickness, highlighting the critical role of CTAB in mesostructure regulation. The synthesis employed TEOS as a high-purity silica precursor with controlled addition via syringe pump over 17 h, enabling the formation of highly defined structures. Such ideal conditions do not reflect the complexity of biomass-derived silica precursors, which contain inorganic impurities and heterogeneous silicate species that may alter CTAB self-assembly, silica condensation kinetics, and pore formation efficiency. The effectiveness of CTAB in biomass-based systems therefore remains insufficiently understood. The present study addresses this limitation by directly evaluating the ability of CTAB to induce mesopore formation in rice husk-derived sodium silicate without complex injection control, providing a more practical approach for scalable mesoporous silica synthesis.

A major limitation of previous studies is the absence of template-free reference materials synthesized under identical conditions, making it difficult to isolate the specific contribution of CTAB to textural modification and adsorption enhancement. Direct comparisons of rice husk-derived SiO_2 synthesized with and without CTAB under identical conditions have not been widely reported, leaving the effects of biomass silica heterogeneity on CTAB templating effectiveness, mesopore formation, and the relationship between surface properties and MB adsorption capacity insufficiently understood. The development of simpler and more energy-efficient synthesis routes using renewable agricultural waste while avoiding expensive organosilicate precursors remains a significant challenge. The present study addresses these gaps through a direct comparison of rice husk-derived mesoporous SiO_2 synthesized with and without CTAB, enabling clearer evaluation of the role of CTAB in pore structure development and adsorption performance. The use of rice husk-derived SiO_2 further supports the development of sustainable and cost-effective mesoporous adsorbents based on renewable resources.

2. Methodology

2.1 Materials

Raw rice husk collected from Tegal, Central Java, Indonesia, was used as the silica (SiO_2) source. Hydrochloric acid (HCl, 37 %; Merck, Germany) and sodium hydroxide (NaOH; Merck, Germany) were employed for the extraction and purification processes. Cetyltrimethylammonium bromide (CTAB; HiMedia Laboratories, India) was used as the structure-directing agent. Deionized water was used throughout all experimental procedures. Methylene blue (MB; Merck, Germany) was selected as the model dye pollutant for adsorption studies.

2.2 Instrument

The structural and physicochemical properties of the SiO_2 materials were characterized by Fourier transform infrared spectroscopy (FTIR, Shimadzu) to identify surface functional groups. Textural properties, including specific surface area, pore volume, and pore size distribution, were determined by gas sorption analysis (GSA, JWGB Sci. & Tech.) based on the Brunauer–Emmett–Teller (BET) method. Surface morphology and elemental composition were examined using scanning electron microscopy coupled with energy-dispersive X-ray spectroscopy (SEM–EDX, JSM-IT700HR). Residual dye concentration after adsorption was quantified by ultraviolet–visible (UV–Vis) spectroscopy using a B-one spectrophotometer.

2.3 Procedure

2.3.1 Extraction of SiO_2 from Rice Husk

Raw rice husk was washed with deionized water and treated with HCl under constant stirring to remove surface impurities and inorganic contaminants, particularly alkali and alkaline earth metal ions that may affect silica purity and pore formation. The treated material was rinsed to neutral pH, filtered, and dried at 80 ℃ for 24 h according to

a previously reported method [10]. The dried rice husk was calcined at 600 ℃ for 2 h to obtain silica ash while preserving the amorphous silica phase, which is more reactive toward alkaline extraction. A total of 5 g of silica ash was mixed with 100 mL of NaOH solution and heated at 90 ℃ for 2 h to produce sodium silicate (Na_2SiO_3). The selected temperature and reaction time were based on literature references and chemical considerations to promote efficient siloxane bond cleavage and silica dissolution. The resulting Na_2SiO_3 solution was cooled to room temperature and filtered to remove insoluble residues, yielding a clear filtrate with a pH of approximately 13 [11].

2.3.2 Synthesis of Mesoporous SiO_2

A total of 0.2 g of CTAB was dissolved in 34 mL of 0.6 N HCl as a structure-directing agent, while a template-free sample was synthesized under identical conditions for comparison. The selected CTAB concentration was based on literature reports indicating sufficient micelle formation for mesoporous self-assembly without excess surfactant accumulation. Acidic conditions were used to promote surfactant homogenization and control the initial reaction rate. The Na_2SiO_3 solution was gradually added to the CTAB solution with pH adjustment to 8, a condition selected to balance silicate hydrolysis and condensation and to facilitate effective interaction between silicate species and CTAB micelles during framework formation. The mixture was aged at 50 ℃ for 24 h to promote gel formation and structural reorganization prior to hydrothermal treatment [12].

The resulting gel was subjected to hydrothermal treatment at 100 ℃ for 48 h to enhance Si–O–Si condensation, improve framework stability, and promote mesopore regularity. The selected hydrothermal conditions were adapted from previous studies, considering energy efficiency and sufficient structural maturation under moderate temperature. The hydrothermal product was filtered, washed to neutral pH, dried at 80 ℃, and calcined at 600 ℃ to remove CTAB and open the mesoporous structure while preserving silica framework integrity [13].

2.3.3 MB Adsorption Test

Adsorption experiments were performed using MB as a model dye to evaluate the effect of contact time. A total of 25 mg of adsorbent was added to 50 mL of MB solution with an initial concentration of 15 mg/L in a 100 mL beaker. The suspension was continuously stirred under dark conditions. Aliquots were collected at predetermined time intervals and centrifuged for 20 minutes. Residual MB concentration was determined by UV–Vis spectrophotometry at the maximum absorption wavelength of 664 nm. Adsorption efficiency and adsorption capacity were calculated using Equation (1) and (2), respectively:

$$\text{Ads. (\%)} = \frac{C_0 - C_e}{C_0} \times 100 \quad (1)$$

$$q_t = \frac{[(C_0 - C_t)] \times v}{w} \quad (2)$$

C_0 and C_e represent the initial and equilibrium MB concentrations (mg/L); q_e denotes the adsorption capacity (mg/g); w corresponds to the adsorbent mass (g); and v represents the solution volume (L) [14].

2.3.4 Adsorption Kinetics

Adsorption kinetic studies were performed to evaluate the adsorption rate and mechanism of MB on MS and MS-CTAB materials. Kinetic analysis was conducted using experimental data obtained from contact experiments under identical conditions [15], with 25 mg of adsorbent dispersed in 50 mL of MB solution. Samples were collected at predetermined time intervals to construct adsorption kinetic profiles. Experimental data were fitted using pseudo-first-order and pseudo-second-order kinetic models, as described by Equations (3) and (4).

$$\ln(q_e - q_t) = \ln q_e - k_1 t \quad (3)$$

$$\frac{t}{q_t} = \frac{1}{K_2 q_e^2} + \frac{1}{q_e} t \quad (4)$$

q_e represents the adsorption capacity at equilibrium (mg/g), q_t denotes the adsorption capacity at time t (mg/g), k_1 and k_2 correspond to the rate constants of the pseudo-first-order and pseudo-second-order kinetic models, respectively, and t represents the contact time (minutes) [11].

2.3.5 Adsorption Isotherms

Adsorption isotherm analysis was performed to evaluate adsorption behavior, maximum adsorption capacity, and adsorbent affinity toward MB [16]. Experiments were conducted using initial MB concentrations of 20, 30, 40, 50, and 60 mg/L, with 25 mg of adsorbent dispersed in 50 mL of solution for both MS and MS-CTAB materials. The suspensions were stirred until equilibrium was reached, followed by determination of residual MB concentration using UV–Vis spectrophotometry.

Langmuir and Freundlich isotherm models were applied to describe adsorption behavior on the prepared materials. The Langmuir model assumes monolayer adsorption on a homogeneous surface [17], whereas the Freundlich model describes adsorption on heterogeneous surfaces [18]. Isotherm parameters were calculated using Equations (5), (6) and (7):

$$\frac{C_e}{q_e} = \frac{1}{q_m} C_e + \frac{1}{K_L . q_m} \quad (5)$$

$$R_L = \frac{1}{1 + K_L C_o} \quad (6)$$

$$\log q_e = \log K_F + \frac{1}{n} \log C_e \quad (7)$$

C_e (mg/L) represents the equilibrium adsorbate concentration in solution (mg/L), q_e denotes the adsorption capacity at equilibrium (mg/g), q_m corresponds to the maximum adsorption capacity (mg/g), K_L is the Langmuir constant related to adsorption affinity (L/mg); R_L represents the separation factor; K_F is the Freundlich constant; n denotes the adsorption intensity constant [19].

Adsorption favorability in the Langmuir model was evaluated using the separation factor (R_L), where $0 < R_L < 1$ indicates favorable adsorption, $R_L > 1$ unfavorable adsorption, $R_L = 1$ linear adsorption, and $R_L = 0$ irreversible adsorption. Surface heterogeneity and adsorption intensity in the Freundlich model were assessed using $1/n$, with $0 < 1/n < 1$ indicating favorable adsorption and $1/n > 1$ indicating unfavorable adsorption [20].

3. Results and Discussion

3.1 Extraction of SiO_2 from Rice Husk

Rice husk-derived SiO_2 was obtained through acid washing, calcination, and alkaline extraction to produce sodium silicate (Na_2SiO_3) as the silica precursor. Acid treatment removed inorganic impurities that may interfere with silicate polymerization, while calcination at 600°C converted the biomass into amorphous silica with high reactivity toward alkaline dissolution. Dissolution of silica ash in NaOH generated soluble silicate species according to Equation (8). Reactive silicate species subsequently underwent hydrolysis and condensation to form a siloxane (Si–O–Si) network [21].

$$SiO_2\,(s) + 2NaOH\,(aq) \rightarrow Na_2SiO_3\,(aq) + H_2O\,(l) \quad (8)$$

Mesoporous structure formation was directed by CTAB, a cationic surfactant that formed micellar aggregates above its critical micelle concentration. Positively charged CTAB micelles acted as soft templates and attracted negatively charged silicate species through a surfactant–inorganic ion-pairing (S^+I^-) mechanism. Gradual addition of Na_2SiO_3 with pH adjustment to 8 promoted balanced silicate hydrolysis and condensation, enabling cooperative self-assembly of silicate species around the micellar surface [12].

Aging at 50 ℃ and hydrothermal treatment at 100 ℃ enhanced structural reorganization, strengthened siloxane bonding, and improved mesophase regularity, resulting in a silica–CTAB composite in which the surfactant occupied the future pore domains [22]. The hydrothermal gel was subsequently washed to neutral pH and dried prior to calcination. Calcination at 600 ℃ removed CTAB through thermal decomposition, generating accessible mesoporous channels corresponding to the space previously occupied by the micelles [12]. Additional condensation of residual silanol groups increased framework rigidity and prevented structural collapse after template removal. Materials synthesized without CTAB underwent uncontrolled silicate condensation, producing less ordered structures with lower pore uniformity and reduced surface area. Template-assisted synthesis therefore promoted more homogeneous mesopore formation and enhanced adsorption accessibility [23]. The synthesis produced two materials, namely mesoporous SiO_2 (MS) and CTAB-templated mesoporous SiO_2 (MS-CTAB), as illustrated in Figure 1.

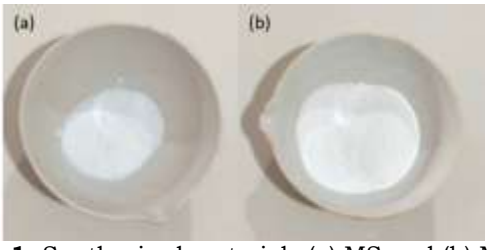

Fig. 1. Synthesized materials (a) MS and (b) MS-CTAB

3.2 FTIR analysis

The FTIR spectra of all samples (Figure 2a-d) exhibited characteristic Si–O–Si absorption bands at approximately 1080–1100 cm^{-1}, 800 cm^{-1}, and 460 cm^{-1}, corresponding to asymmetric stretching, symmetric stretching, and bending vibrations of the siloxane framework, confirming successful SiO_2 formation [24]. Broad absorption bands at approximately 3400 cm^{-1} and 1630 cm^{-1} were assigned to silanol (Si–OH) groups and adsorbed water, indicating the presence of surface hydroxyl groups involved in silicate condensation and pore development [25]. The MS-CTAB sample before calcination (Figure 2c) showed additional absorption bands at 2920–2850 cm^{-1} and 1470–1380 cm^{-1}, attributed to the C–H stretching and bending vibrations of CTAB alkyl chains, confirming successful surfactant incorporation during the self-assembly process. Increased intensity in these regions reflected the presence of organic template species embedded within the silica matrix [26].

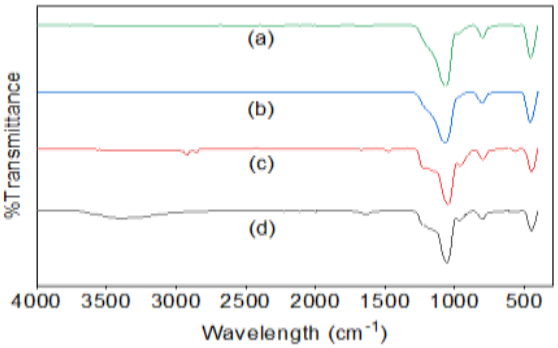

Fig. 2. FTIR spectra of (a) MS before calcination (b) MS after calcination (c) MS-CTAB before calcination and (d) MS-CTAB after calcination

The disappearance of CTAB-related bands after calcination (Figure 2d) confirmed effective surfactant removal and successful template extraction. Reduced intensity of the hydroxyl-related bands at 3400 cm^{-1} and 1630 cm^{-1} indicated further condensation of silanol groups into Si–O–Si linkages, suggesting enhanced framework crosslinking and improved pore wall stability [27]. Slight sharpening and increased definition of the Si–O–Si bands after calcination further supported structural consolidation of the silica network. FTIR results therefore support the proposed formation mechanism, in which CTAB served as a temporary structure-directing agent that guided mesopore formation before thermal removal generated accessible open-pore channels [7].

3.3 BET Analysis

The N_2 adsorption–desorption isotherm of untemplated mesoporous SiO_2 is presented in Figure 3(a). The isotherm exhibited a gradual increase in adsorption at low relative pressure ($p/p_0 < 0.2$), followed by a continuous rise toward $p/p_0 \approx 1.0$. This adsorption behavior corresponds to a type IV isotherm according to IUPAC classification, indicating the presence of mesoporous structures [28]. Relatively low N_2 uptake suggested limited surface area and pore volume. A narrow and weakly

developed hysteresis loop reflected irregular pore geometry and possible interparticle aggregation, indicating less controlled pore formation in the absence of a template [29].

The N_2 adsorption–desorption isotherm of CTAB-templated mesoporous SiO_2 is shown in Figure 3(b). A similar type IV isotherm was observed, accompanied by significantly higher adsorption capacity over the entire relative pressure range. A pronounced increase in adsorption at intermediate to high p/p_0 indicated enhanced capillary condensation within the mesoporous channels [28]. A well-defined hysteresis loop resembling the H1 type suggested the presence of cylindrical pores with relatively uniform size distribution, confirming the formation of a more ordered mesoporous framework directed by the CTAB template [30].

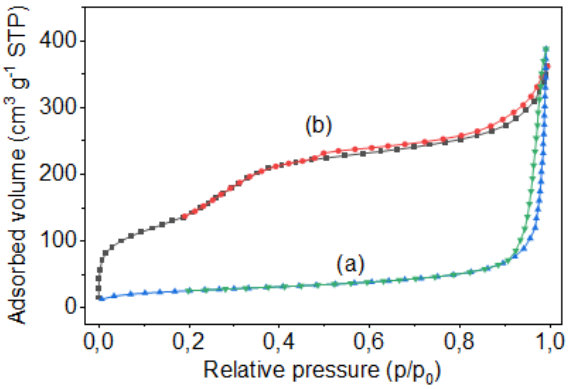

Fig. 3. (a) N_2 adsorption–desorption isotherms of (a) MS and (b) MS-CTAB

3.4 Pore Size Distribution Analysis

The pore size distribution curve of untemplated mesoporous SiO_2, presented in Figure 4(a), exhibited a broad and irregular profile without a distinct dominant peak within the mesoporous region. Fluctuations at larger pore diameters suggested heterogeneous pore sizes, likely associated with interparticle voids and structural defects caused by particle aggregation. The absence of a well-defined distribution indicated limited control over pore development during template-free synthesis [29].

The pore size distribution of CTAB-templated mesoporous SiO_2, shown in Figure 4(b), displayed a sharp and dominant peak within the pore diameter range of approximately 2–4 nm. A narrow and symmetric distribution of pore volume (dV/dD) indicated high pore uniformity and successful formation of a homogeneous mesoporous structure. Predominance of pores within the lower mesoporous range demonstrated the effectiveness of CTAB as a structure-directing agent through a stable templating mechanism during synthesis [30]. Textural characterization further revealed a substantial increase in specific surface area from 89.63 m^2/g for MS to 580.38 m^2/g for MS-CTAB, highlighting the significant influence of CTAB on pore development and surface accessibility [31].

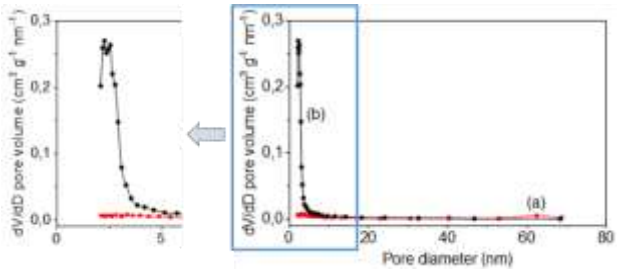

Fig. 4. (a) Pore size distribution curves of (a) MS and (b) MS-CTAB

3.5 SEM-EDX Analysis

SEM micrographs recorded at 10,000× magnification revealed distinct differences in the surface morphology and particle organization of MS and MS-CTAB. The untemplated MS sample (Figure 4a) exhibited closely packed silica domains with limited interparticle voids, indicating a more compact structural arrangement [29]. EDX analysis confirmed the predominance of Si and O as the principal elemental constituents, with mass compositions of 54.91 % and 45.09 %, respectively. Elemental mapping showed homogeneous distribution of both elements across the material surface, confirming the formation of a relatively pure SiO_2 framework without detectable residual organic species.

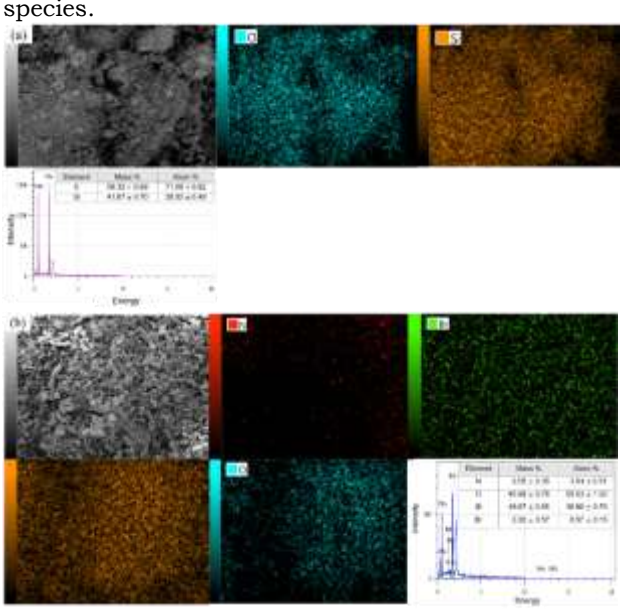

Fig. 5. (a) SEM micrographs and EDX elemental mapping of (a) MS and (b) MS-CTAB, recorded at 10,000× magnification

The MS-CTAB sample displayed a more separated particle arrangement with more distinguishable interparticle spaces, reflecting the influence of CTAB on silica organization during synthesis [29]. EDX analysis identified Si and O as the major components, accompanied by minor N and Br signals attributed to residual CTAB species. Homogeneous distribution of Si, O, N, and Br further supported the incorporation of CTAB as a structure-directing agent during the self-assembly process. Morphological differences between MS and MS-CTAB, together with BET results showing increased

surface area and improved pore size distribution, indicate that CTAB-assisted synthesis promoted enhanced structural accessibility and more ordered mesopore development [30]. Improved accessibility of adsorption sites likely facilitated more efficient diffusion of MB molecules and contributed to the higher adsorption capacity observed for MS-CTAB.

3.6 Standard Curve Measurement

The calibration curve was established using MB standard solutions with concentrations of 1, 2, 3, 4, 5, and 6 ppm. Absorbance was measured at the maximum absorption wavelength, and the resulting data were plotted with concentration as the independent variable and absorbance as the dependent variable. Linear regression analysis yielded the equation y = 0.1242x + 0.0115 with a coefficient of determination (R^2) of 0.9988 indicating excellent linearity. The obtained regression equation was subsequently used to determine the MB concentration in the adsorption samples [32].

3.7 Adsorption Kinetics

The adsorption profiles presented in Figure 6 demonstrate a progressive increase MB removal with increasing contact time until equilibrium was achieved. Equilibrium adsorption percentages obtained from triplicate measurements were 74.19 ± 0.70 % for MS and 86.02 ± 0.39 % for MS-CTAB, confirming the improved adsorption performance of the CTAB-templated material. Enhanced adsorption efficiency in MS-CTAB was attributed to the increased effectiveness of CTAB-assisted mesostructural modification [33]. BET analysis showed that MS-CTAB possessed a significantly higher specific surface area (580.38 m^2/g) than MS (89.63 m^2/g), providing a greater number of accessible adsorption sites for MB molecules [34].

Surface chemistry plays a crucial role in adsorption performance. Surface silanol (Si–OH) groups on silica act as active adsorption sites through hydrogen bonding and electrostatic interactions with cationic MB molecules. The surface charge of silica is strongly pH-dependent due to protonation and deprotonation of silanol groups. Under near-neutral to alkaline conditions, partial deprotonation can generate negatively charged siloxide species ($Si–O^-$), thereby enhancing electrostatic attraction toward positively charged MB molecules. Adsorption behavior is governed not only by textural properties such as surface area and pore accessibility but also by surface chemistry, particularly functional groups that control adsorbent–adsorbate interactions [35].

Kinetic fitting results shown in Figure 7 indicate that the pseudo-first-order model yielded lower correlation coefficients, with R^2 values of 0.8864 for MS and 0.9599 for MS-CTAB, suggesting limited suitability for describing the adsorption behavior of MB on both materials. Pseudo-first-order rate constants were comparable, with k_1 values of 0.12 min^{-1} for MS and 0.12 min^{-1} for MS-CTAB, indicating similar initial adsorption rates. The pseudo-second-order model provided better agreement with the experimental data, as reflected by higher correlation coefficients and close correspondence between calculated adsorption capacities (q_{cal}) (22.83 mg/g for MS and 26.18 mg/g for MS-CTAB) and experimental values (q_{exp}) (22.26 mg/g and 25.80 mg/g). The higher pseudo-second-order rate constant (k_2) observed for MS-CTAB (0.0462 g mg^{-1} min^{-1}) relative to MS (0.0367 g mg^{-1} min^{-1}) indicates accelerated adsorption kinetics following CTAB modification [33].

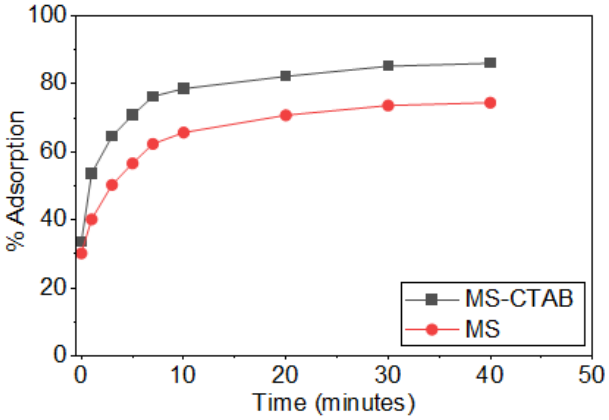

Fig. 6. Effect of contact time on MB adsorption

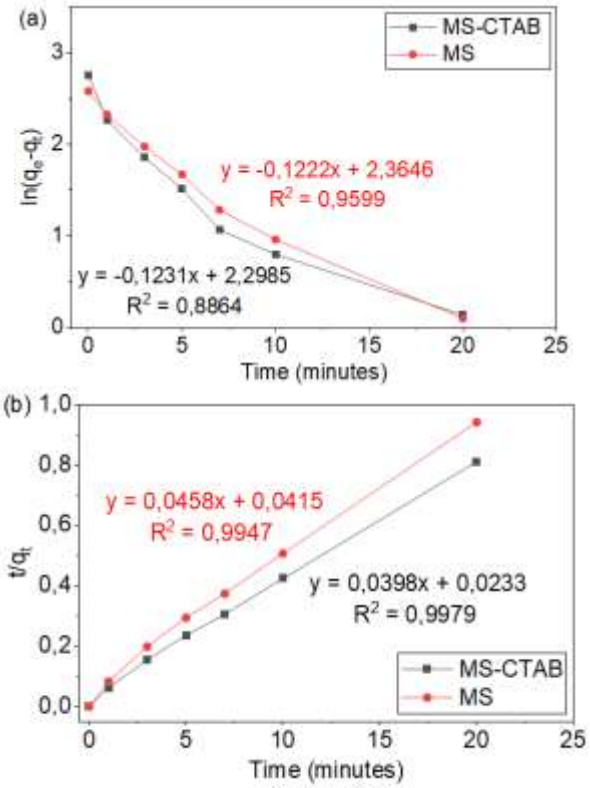

Fig. 7. Adsorption kinetics of MB on MS and MS-CTAB (a) pseudo-first-order kinetics; (b) pseudo-second-order kinetics

The pseudo-second-order model provided a better fit to the experimental data than the pseudo-first-order model, as indicated by the higher correlation coefficients and the close agreement between calculated and experimental adsorption capacities [36]. These results suggest that the adsorption rate was strongly influenced by adsorbate uptake capacity and surface interaction processes. The applicability of the pseudo-second-order model

should not be interpreted as definitive evidence of chemisorption, as similar kinetic behavior may also be observed in physically driven adsorption systems. Contributions from external mass transfer and intraparticle diffusion cannot be excluded and may influence the overall adsorption process; however, further diffusion-based kinetic analysis would be required to determine the dominant rate-controlling mechanism. The enhanced adsorption performance of MS-CTAB is attributed to the combined effects of increased surface area, improved pore accessibility, and favorable interactions between silanol groups and MB molecules, demonstrating the effectiveness of CTAB-assisted mesostructural modification in improving adsorption functionality [35].

3.8 Adsorption Isotherm Analysis

The adsorption behavior of MB on MS-CTAB was evaluated using the Langmuir and Freundlich isotherm models to examine both adsorption capacity and surface interaction characteristics. Linear fitting results presented in Figure 8 showed that the Langmuir model provided a higher correlation coefficient (R^2 = 0.9847) than the Freundlich model (R^2 = 0.8998), indicating that Langmuir better described the overall adsorption equilibrium. The Langmuir model assumes monolayer adsorption on energetically equivalent adsorption sites [17]. A maximum adsorption capacity (q_{max}) of 63.29 mg/g was obtained, indicating substantial MB uptake for a biomass-derived SiO_2-based adsorbent, suggesting effective adsorption performance with relatively simple surface modification.

The Langmuir affinity constant (K_L) of 0.3050 L/mg reflects the affinity between the adsorbent surface and MB molecules, suggesting favorable adsorption even at relatively low equilibrium concentrations. The dimensionless separation factor (R_L) remained within the range $0 < R_L < 1$, confirming that the adsorption process was thermodynamically favorable and readily attainable across the investigated concentration range. Residual structural irregularities, non-uniform silanol distribution, and variations in pore accessibility may introduce heterogeneous adsorption environments that are not fully represented by the Langmuir assumptions. The Freundlich model, which describes multilayer adsorption on heterogeneous surfaces, yielded a K_F value of 24.27, indicating substantial adsorption capacity, while the 1/n value within the range $0 < 1/n < 1$ confirmed favorable adsorption intensity and strong adsorbate–adsorbent interactions [20].

Superior Langmuir fitting suggests that MB adsorption predominantly occurred through monolayer coverage on relatively accessible and energetically similar adsorption sites, likely associated with the uniform mesoporous structure generated by CTAB templating. Contribution of heterogeneous adsorption cannot be completely excluded, particularly considering the biomass origin of the silica and the presence of surface silanol groups with varying local environments. Adsorption behavior in this system is therefore more realistically described as predominantly Langmuir, with partial heterogeneity reflected by the Freundlich parameters. Combined interpretation of q_{max}, K_L, R_L, and Freundlich constants indicates that the enhanced adsorption performance of MS-CTAB was governed not only by increased adsorption capacity but also by favorable surface affinity, accessible mesoporous pathways, and chemically active silanol sites capable of interacting effectively with MB molecules [17].

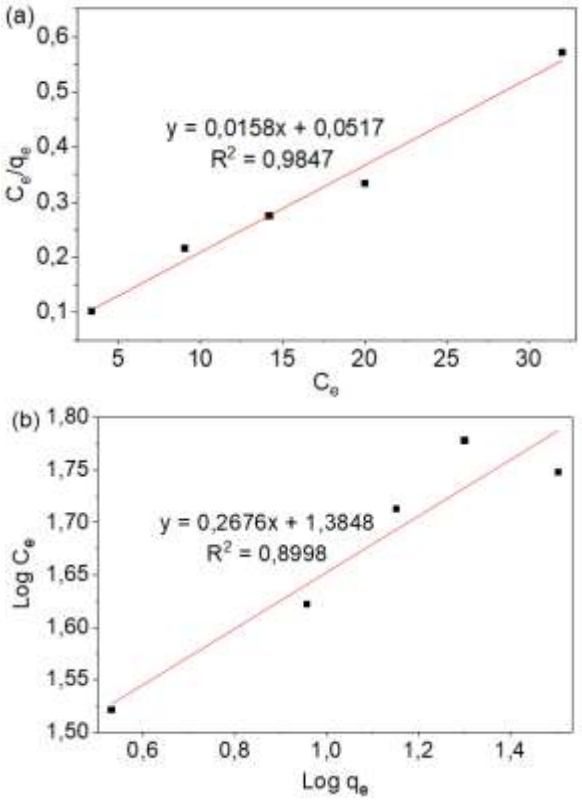

Fig. 8. Adsorption isotherm curves (a) Langmuir; (b) Freundlich

According to Table 1, the q_{max} of MS-CTAB reached 63.29 mg/g, indicating competitive adsorption performance compared with previously reported silica-based adsorbents. Previously reported adsorbents with comparable or higher capacities were generally synthesized using commercial organo-silicate precursors, multi-step functionalization, or composite systems, which may increase production cost and limit large-scale application. The present study utilized rice husk-derived sodium silicate as a renewable silica precursor, adding value through agricultural waste valorization and reducing dependence on commercial silica sources. The synthesis employed a simple CTAB-assisted hydrothermal method under moderate conditions (100 ℃) without complex precursor modification or multistep composite fabrication [7]. CTAB-assisted template formation improved surface area, pore accessibility, and adsorption affinity while maintaining a straightforward preparation strategy. Structural stability after calcination supports potential reusability and operational durability for wastewater treatment applications. The combination of competitive adsorption capacity, low-cost biomass

precursor, and simplified synthesis highlights the practical significance of MS-CTAB as a promising mesoporous adsorbent for sustainable dye removal [37].

Table 1. Comparison of q_{max} of various SiO_2 -based adsorbents

Materials	q_{max} (mg/g)	References
$P@SiO_2$	76.92	[38]
Mesoporous-SiO_2	71.40	[27]
SFH-SiO_2	70.16	[39]
Fe_3O_4-SiO_2	40.00	[8]
PVP-SiO_2-D	30.40	[40]
SiO_2 /PANI-SDS	24.90	[41]
MS-CTAB	63.29	This work

4. Conclusion

Mesoporous SiO_2 (MS) and CTAB-templated mesoporous SiO_2 (MS-CTAB) were successfully synthesized from rice husk-derived sodium silicate via a hydrothermal method, demonstrating the conversion of agricultural waste into value-added adsorbent materials. Structural characterization confirmed the role of CTAB in directing mesopore formation, increasing specific surface area from 89.63 m^2/g to 580.38 m^2/g, along with improved pore uniformity and surface accessibility. Adsorption performance evaluation showed higher MB removal efficiency for MS-CTAB (86.02 ± 0.39 %) compared with MS (74.19 ± 0.70 %), attributed to enhanced textural properties and surface interactions involving silanol groups that facilitate hydrogen bonding and electrostatic attraction. Kinetic analysis indicated that the pseudo-second-order model best described the adsorption process, suggesting that adsorption was governed by surface interaction and adsorption capacity. Isotherm analysis revealed that MB adsorption followed the Langmuir model with q_{max} of 63.29 mg/g, indicating monolayer adsorption on accessible adsorption sites. Overall performance, combined with biomass-derived precursor utilization and a relatively simple synthesis route, highlights the potential of MS-CTAB as a sustainable adsorbent for dye-contaminated wastewater treatment. CTAB-assisted mesostructural engineering effectively enhances the functional properties of biomass-based mesoporous silica materials.

Acknowledgment

The authors would like to thank Diponegoro University for its financial support for this research through the 2025 PNPB funding scheme (Contract No. 222-501/UN7.D2/PP/IV/2025).

References

[1] Kishor, R., Purchase, D., Saratale, G. D., Saratale, R. G., Ferriera, L. F. R., Bilal, M., Chandra, R., & Bharagava, R. N. (2021). Ecotoxicological and health concern of persistent pollutants. *Journal of Environmental Chemical Engineering, 9*(2), 105012. https://doi.org/10.1016/j.jece.2020.105012

[2] Mo, H., Liu, L., Yang, Z., Lao, Y., & He, Y. (2025). The effect of magnesium oxide on the structure of metakaolin-based geopolymer microspheres and its application in the adsorption of methylene blue dye. *Journal of Water Process Engineering, 70*, 106937. https://doi.org/10.1016/j.jwpe.2025.106937

[3] Shindhal, T., Rakholiya, P., Varjani, S., Pandey, A., Ngo, H. H., Guo, W., Ng, H. Y., & Taherzadeh, M. J. (2020). A critical review on advances in the practices and perspectives for the treatment of dye industry wastewater. *Bioengineered, 12*(1), 70–87. https://doi.org/10.1080/21655979.2020.1863034

[4] Mane, S. M., Raorane, C. J., & Shin, J. C. (2022). Synthesis of mesoporous silica adsorbent modified with mercapto–amine groups for selective adsorption of Cu^{2+} ion from aqueous solution. *Nanomaterials, 12*, 3232. https://doi.org/10.3390/nano12183232

[5] Yan, L., Zhou, K., Zhang, R., & Zhu, X. (2023). Efficient adsorption of anionic azo dye in wastewater with medulla tetrapanacis modified by cationic surfactant. *Water, Air, & Soil Pollution, 234*(8). https://doi.org/10.1007/s11270-023-06464-9

[6] Ijaz, S., Kausar, A., Iqbal, M., Messaoudi, N. E., Miyah, Y., Knani, S., & Graba, B. (2025). Advances in extraction of silica from rice husk and its modification for environmentally friendly wastewater treatment via adsorption technology. *Journal of Water Process Engineering, 71*, 107187. https://doi.org/10.1016/j.jwpe.2025.107187

[7] Subhan, F., Aslam, S., Yan, Z., Yaseen, M., Naeem, M., Ikram, M., Ali, A., & Bibi, S. (2022). Adsorption and reusability performance of hierarchically porous silica (MMZ) for the removal of MB dye from water. *Inorganic Chemistry Communications, 139*, 109380. https://doi.org/10.1016/j.inoche.2022.109380

[8] Ali, N. S. M., Lalwan, H. A., Alminshid, A. H., & Mohammed, M. M. (2022). Synthesis and characterization of Fe_3O_4–SiO_2 nanoparticles as adsorbent material for methyl blue dye removal from aqueous solutions. *Pollution, 8*(1), 295–302. https://doi.org/10.22059/POLL.2021.328697.1157

[9] Kim, Y. S., & An, G. S. (2025). Surface engineering of Fe_3O_4@SiO_2 core–shell nanoparticles: Role of CTAB/TEOS ratio. *Ceramics International, 51*, 379–385. https://doi.org/10.1016/j.ceramint.2024.11.006

[10] Castillo, J., Vargas, V., Macero, D., Beulze, A. L., Ruiz, W., & Bouy, B. (2021). One-step synthesis of SiO_2 α-Fe_2O_3/Fe_3O_4 composite nanoparticles with magnetic properties from rice husks. *Physica B: Condensed Matter, 605*, 412799. https://doi.org/10.1016/j.physb.2020.412799

[11] Ulfa, M., Prasetyoko, D., Trisunaryanti, W.,

Bahruji, H., Fadila, Z. A., & Sholeha, N. A. (2022). The effect of gelatin as pore expander in green synthesis mesoporous silica for methylene blue adsorption. *Scientific Reports, 12*, 19615. https://doi.org/10.1038/s41598-022-19615-5

[12] Li, H., Wang, W., Wang,L., Chen, L., & Liu, C. (2025). Framework Zr-enriched hierarchical Zr-Si zeolites photocatalysts: Effects and mechanism of CTAB amount on photocatalytic performance. *Journal of Alloys and Compounds, 1013*, 178563. https://doi.org/10.1016/j.jallcom.2025.178563

[13] Trisunaryanti, W., & Triyono. (2022). *Katalis cerdas bermatriks material mesopori tercetak gelatin: Sintesis dan aplikasinya*. Yogyakarta: Gadjah Mada University Press. https://ugmpress.ugm.ac.id/id/product/kimia/katalis-cerdas-bermatriks-material-mesopori-tercetak-gelatin-sintesis-dan-aplikasinya

[14] Khanna, S., Kiruthika, M., Chidambaram, S., & Rathinam, M. (2023). Preparation of hierarchical self-assembled SiO_2/ZnO composite by low-temperature hydrothermal approach for enhanced adsorption of 4-nitrophenol and dyes. *Materials Science and Engineering B, 293*, 116484. https://doi.org/10.1016/j.mseb.2023.116484

[15] Hamad, H. N., & Idrus, S. (2022). Recent developments in the application of bio-waste-derived adsorbents for the removal of methylene blue from wastewater: A review. *Polymers, 14*, 783. https://doi.org/10.3390/polym14040783

[16] Zhu, Y., Cui, Y., Peng, Y., Dai, R., Chen, H., & Wang, Y. (2023). Preparation of CTAB intercalated bentonite for ultrafast adsorption of anionic dyes and mechanism study. *Colloids and Surfaces A: Physicochemical and Engineering Aspects, 658*, 130705. https://doi.org/10.1016/j.colsurfa.2022.130705

[17] Sarwar, A., Wang, J., Khan, M. S., Farooq, U., Riaz, N., Nazir, A., Mahmood, Q., Hashem, A., Al-Arjani, A. B. F., Alqarawi, A. A., & Abd_Allah, E. F. (2021). Iron oxide (Fe_3O_4)-supported SiO_2 magnetic nanocomposites for efficient adsorption of fluoride from drinking water: Synthesis, characterization, and adsorption isotherm analysis. *Water, 13*(11), 1514. https://doi.org/10.3390/w13111514

[18] Al-mahmodi, A. F., Atta, M. R., Munusamy, Y., & Al-dhawi, B. N. S. (2025). Adsorption of reactive black 5 dye using eggshell waste supported by Fe_2O_3: An equilibrium isotherms study. *Chemical Thermodynamics and Thermal Analysis, 18*, 100174. https://doi.org/10.1016/j.ctta.2025.100174

[19] Saod, W. M., Oliver, I. W., Contini, A., & Zholobenko, V. (2025). Synthesis and characterisation of an iron oxide mesoporous silica nano-composite and its application in removal of methylene blue dye. *Journal of Molecular Structure, 1319*, 139390. https://doi.org/10.1016/j.molstruc.2024.139390

[20] Mrosso, R., Mecha, A. C., & Kiplagat, J. (2024). Performance evaluation of calcined eggshell waste (sorbent) for biogas upgrading: Adsorption isotherms, adsorption kinetics, and fixed bed studies. *Environmental Challenges, 16*, 100961. https://doi.org/10.1016/j.envc.2024.100961

[21] Liu, S., Wang, B., Jin, S., Zhang, L., Yang, Z., Wu, Y., & Gao, S. (2025). Silicone resin-based covalent adaptive networks additionally cross-linked by Si–O–Ph bonds. *ACS Sustainable Chemistry & Engineering, 13*. https://doi.org/10.1021/acssuschemeng.4c08061

[22] Vu, A. T., Xuan, T. N., & Lee, C. H. (2019). Preparation of mesoporous Fe_2O_3·SiO_2 composite from rice husk as an efficient heterogeneous Fenton-like catalyst for degradation of organic dyes. *Journal of Water Process Engineering, 28*, 10–19. https://doi.org/10.1016/j.jwpe.2019.01.019

[23] Ye, Z., Chen, C., Su, Y., Feng, J., & Yin, Y. (2025). Templating methods for materials fabrication across scales. *Chemical Reviews, 126*(2). https://doi.org/10.1021/acs.chemrev.4c00633

[24] Widiyandari, H., Pardoyo, P., Sartika, J., Putra, O. A., Purwanto, A., & Ernawati, L. (2021). Synthesis of mesoporous SiO_2 xerogel from geothermal sludge using sulfuric acid as gelation agent. *International Journal of Engineering, 34*(7), 1569–1575. https://doi.org/10.5829/ije.2021.34.07a.05

[25] Arsyad, W. S., Lisar, M. G., Ramadhan, L. O. A. N., & Usman, I. (2024). Green synthesis nanopartikel perak dari buah naga merah (Hylocereus polyrhizus) dan karakterisasi sifat fisika dan kimianya sebagai penyerap cahaya dalam sel surya DSSC. *Jurnal Aplikasi Fisika, 20*(1), 1–15. https://doi.org/10.62749/jaf.v20i01.p1-15

[26] Ananda, A., & Aini, S. (2021). Sintesis silika mesopori menggunakan bahan dasar Na_2SiO_3 yang dihasilkan dari pasir silika dengan metoda hidrotermal. *Chemistry Journal of State University of Padang, 10*(1). https://doi.org/10.24036/cjou.v10i1.115

[27] Samy, A., Ismail, A. M., & Ali, H. (2023). Environmentally friendly mesoporous SiO_2 with mixed fiber/particle morphology and large surface area for enhanced dye adsorption. *Journal of Materials Science, 58*, 1586–1607. https://doi.org/10.1007/s10853-022-08119-2

[28] Niu, Y., Bao, W., Li, Y., Liu, X., & Tian, Y. (2026). Investigation of Fe_2O_3@SiO_2 catalysts synthesized via various methods for the catalytic gasification of pinewood. *Renewable Energy, 256*, 124096. https://doi.org/10.1016/j.renene.2025.124096

[29] Ajayi, S. M., Olusanya, S. O., Abimbade, S. F., Olumayede, E. G., & Faboya, O. L. (2025). Surface morphology and textural properties of

mesoporous silica materials prepared from agricultural waste. *Next Research, 2*, 100758. https://doi.org/10.1016/j.nexres.2025.100758

[30] Calzaferri, G., Gallagher, S. H., Lustenberger, S., Walther, F., & Brühwiler, D. (2023). Multiple equilibria description of type H1 hysteresis in gas sorption isotherms of mesoporous materials. *Materials Chemistry and Physics, 296*, 127121. https://doi.org/10.1016/j.matchemphys.2022.127121

[31] Enrique, B., Escobar, V., Díaz, D., García-Peña, N. G., & Redón, R. (2025). Amorphous and crystalline SiO_2 supports interaction with ZnO obtained by various methods: Implications for rhodamine 6G elimination. *Journal of Coordination Chemistry, 78*(20), 2251–2270. https://doi.org/10.1080/00958972.2025.2566367

[32] Bimala, A. R. F., Indrasari, T., & Maritha, V. (2025). Validasi metode analisis rhodamin-B pada saos tomat menggunakan spektrofotometri UV-Vis. *Jurnal Borneo Saintek, 8*(2), 59–64. https://doi.org/10.62749/jaf.v20i01.p1-15

[33] Ulfa, M., Nur, C., & Amalia, N. (2023). Fine-tuning mesoporous silica properties by a dual-template ratio as TiO_2 support for dye photodegradation booster. *Heliyon, 9*(6), e16275. https://doi.org/10.1016/j.heliyon.2023.e16275

[34] Yap, P. L., Wang, D., & Losic, D. (2025). Advancing methylene blue adsorption approach for more precise measurement of specific surface area of graphene oxide. *Advanced Materials Interfaces, 12*. https://doi.org/10.1002/admi.202500214

[35] Kyriakopoulos, G. L., Tsimnadis, K., Sebos, I., & Charabi, Y. (2024). Investigating the effect of pore size distribution on the sorption types and the adsorption-deformation characteristics of porous continua: The case of adsorption on carbonaceous materials. *Crystals, 14*, 742. https://doi.org/10.3390/cryst14080742

[36] Hachemaoui, M., Boukoussa, B., Mokhtar, A., Mekki, A., Beldjilali, M., Benaissa, M., Zaoui, F., Hakiki, A., Chaibi, W., Sassi, M., & Hamacha, R. (2020). Dyes adsorption, antifungal and antibacterial properties of metal loaded mesoporous silica: Effect of metal and calcination treatment. *Materials Chemistry and Physics, 256*, 123704. https://doi.org/10.1016/j.matchemphys.2020.123704

[37] Singh, S., & Kumar, N. (2024). Removal of dyes from wastewater using low-cost adsorbents. *Macromolecular Symposia*. https://doi.org/10.1002/masy.202400156

[38] Nayl, A. A., Abd-Elhamid, A. I., Arafa, W. A. A., Ahmed, I. M., Abdel-Rahman, A. M. E., Soliman, H. M. A., Abdelgawad, M. A., Ali, H. M., Aly, A. A., & Bräse, S. (2023). A novel P@SiO_2 nano-composite as effective adsorbent to remove methylene blue dye from aqueous media. *Scientific Reports, 13*, 18054. https://doi.org/10.1038/s41598-023-45344-4

[39] Aldabagh, I. S., Neithal, D., & Ahmed, E. I. (2024). Removal of methylene blue from aqueous solution by green synthesized silicon dioxide nanoparticles using sunflower husk. *Chemical Engineering Journal Advances, 18*, 100608. https://doi.org/10.1016/j.ceja.2024.100608

[40] Zhu, W., Wu, Z., Zhao, S., Lv, F., Zhang, Y., & Guo, S. (2023). Selective adsorption and separation of methylene blue from wastewater by self-standing polyvinylpyrrolidone and SiO_2 electrospun membranes. *Chemical Engineering Science, 280*, 119009. https://doi.org/10.1016/j.ces.2023.119009

[41] Salem, M. A., Salem, I. A., El-Dahrawy, W. M., & El-Ghobashy, M. A. (2023). Nano-silica from white silica sand functionalized with PANI-SDS (SiO_2/PANI-SDS) as an adsorbent for the elimination of methylene blue from aqueous media. *Scientific Reports, 13*, 1–17. https://doi.org/10.1038/s41598-023-45873-y